NOAA Technical Memorandum OAR PMEL-140

CHARACTERIZING THE INTERANNUAL VARIABILITY OF THE EQUATORIAL PACIFIC: AN OLR PERSPECTIVE

Andrew M. Chiodi[1,2]
D.E. Harrison[1,2]

[1]Joint Institute for the Study of the Atmosphere and Ocean (JISAO)
University of Washington, Seattle, WA

[2]Pacific Marine Environmental Laboratory
Seattle, WA

Pacific Marine Environmental Laboratory
Seattle, WA
June 2008

UNITED STATES DEPARTMENT OF COMMERCE

Carlos M. Gutierrez
Secretary

NATIONAL OCEANIC AND ATMOSPHERIC ADMINISTRATION

VADM Conrad C. Lautenbacher, Jr.
Under Secretary for Oceans and Atmosphere/Administrator

Office of Oceanic and Atmospheric Research

Richard W. Spinrad
Assistant Administrator

NOTICE from NOAA

Mention of a commercial company or product does not constitute an endorsement by NOAA/OAR. Use of information from this publication concerning proprietary products or the tests of such products for publicity or advertising purposes is not authorized. Any opinions, findings, and conclusions or recommendations expressed in this material are those of the authors and do not necessarily reflect the views of the National Oceanic and Atmospheric Administration.

Contribution No. 3204 from NOAA/Pacific Marine Environmental Laboratory

Also available from the National Technical Information Service (NTIS)
(`http://www.ntis.gov`)

Contents

Characterizing the interannual variability of the equatorial Pacific: An OLR perspective

A.M. Chiodi[1,2] and E.D. Harrison[1,2]

Abstract. There has been considerable societal importance placed on the ability to distinguish and predict interannual anomalies of the tropical Pacific's coupled ocean-atmosphere system. Specific importance has been placed on determining when anomalous conditions follow one of two sets of conditions first described in detail by Bjerknes and commonly referred to as "El Niño" and "La Niña." Here, we investigate the use of outgoing-longwave-radiation (OLR) as a means of determining "El Niño"-type anomalies operationally and retrospectively. We find that OLR, averaged over regions which are known to play a role in Bjerknes feedbacks over the tropical Pacific, can be used to unambiguously identify such interannual anomalies and that some OLR-based indices are advantageous in terms of the degree to which anomalous years are clearly distinguished from background variability. Thus, OLR offers a useful perspective on the state of the coupled tropical Pacific system and should be considered when assessing the state of this system, along with other more traditionally discussed variables such as sea surface temperature (SST) and sea level pressure (SLP).

1. Introduction

Coupled ocean-atmosphere processes are known to cause variability on a range of temporal and spatial scales in the equatorial Pacific. Considerable societal importance, however, has been attached specifically to determining occasions in which the interannual variability of the system follows a set of conditions first described in detail by Bjerknes, commonly referred to as El Niño-Southern Oscillation (ENSO) events.

The ENSO phenomenon has become familiar around the world because substantial weather anomalies often occur during periods of extreme "ENSO-state." The warm and cold phases of ENSO, generally referred to as El Niño and La Niña, respectively, often bring anomalous regional rainfall and sometimes anomalous seasonal temperatures. Lists of years of extreme conditions have been composited and multi-month life cycles of "El Niño events" and "La Niña events," as well as associated weather anomalies, have been constructed and evaluated for the robustness of the characteristic weather anomalies (see Ropelewski and Halpert, 1987, 1996; Trenberth and Caron, 2000; Harrison and Larkin, 1998; Smith *et al.*, 1999) Such composites provide a statistical basis for seasonal weather forecasting in the affected regions, if the statistical linkages are sufficiently strong. The dynamical basis for such relationships is based on the fact that extremes of ENSO involve substantially anomalous patterns of deep tropical convection and, hence, of large-scale atmospheric forcing that can be expected to drive tropical and extra-tropical atmospheric circulation anomalies.

Traditionally, the occurrence of such anomalies has been agreed upon based on qualitative considerations. There is, however, a need to unambigu-

[1]Joint Institute for the Study of the Atmosphere and Ocean, University of Washington, Seattle, WA

[2]NOAA, Pacific Marine Environmental Laboratory, Seattle, WA

ously determine both previous and future events from simple observational metrics. In the past decade or two, indices based on sea surface temperature (SST) and sea level pressure (SLP) difference have commonly served this purpose. Multivariate ENSO indices, e.g., the Bjerknes ENSO Index (BEI, see Harrison and Larkin, 1996) and the Multivariate ENSO index (Wolter and Timlin, 1998) have also been proposed but have not gained wide acceptance (reference indices shown for period 1950–2007 in Appendix A.) Here, we evaluate a different readily observed variable in terms of its ability to clearly distinguish years in which significantly anomalous conditions occur on interannual timescales. We find that outgoing-longwave-radiation (OLR), averaged over a region known to play a role in Bjerknes feedbacks over the tropical Pacific, can be used to unambiguously identify interannual anomalies related to warm-ENSO, and that this OLR-based index is advantageous in terms of the (1) degree to which anomalous years are clearly distinguished from background variability, (2) the ability to directly interpret changes in OLR as significant phenomenological changes in the coupled tropical Pacific system (i.e., the presence of atmospheric deep convection), and (3) the usefulness of absolute monthly data, as opposed to longer-term anomaly averages.

From an operational perspective, the detection and identification of significant shifts in the coupled tropical Pacific system depends upon first quantifying the "normal" or background variability of the system. In this context, an ideal index will be one in which the events of main interest (significant phenomenological anomalies) are clearly distinct from the observed background variability. Furthermore, these outliers should be indicative of fundamental phenomenological shifts in the system's behavior. Thus, we investigate the extent to which the metrics considered here have unambiguous (statistically significant) outliers that occur on interannual timescales and are indicative of fundamental-phenomenological shifts (i.e., Bjerknes conditions) in the system. Herein, we will statistically distinguish between background and outlier by comparing observations to a commensurate "normal" (Gaussian) system (described below).

First, it is helpful to review some well-known average conditions of the tropical Pacific. Normally, relatively strong easterlies are present over the central equatorial Pacific. These easterlies depress the thermocline in the West, shoal the thermocline in the East, and drive upwelling, which leads to the formation of a cold-tongue of SST in the central and eastern equatorial Pacific. This creates a gradient in SST between the warm western and cooler central and eastern tropical Pacific. This gradient is involved in setting up a SLP gradient between the eastern (high SLP) and western (low SLP) tropical Pacific, which in turn is involved in driving the Walker Circulation, in which air flows west along the equator, rises over the western Pacific and Maritime Continent, is returned to the east in the upper troposphere, and sinks over the eastern Pacific. Accordingly, the central and eastern tropical Pacific is normally arid while heavy rains occur over the (convective) western tropical Pacific.

Bjerknes (1969) proposed that the strong interannual variability of this system can be explained by sequences of positive feedbacks which push the

system into one of two phases. For example, if wind anomalies over the equatorial Pacific lead to warming of the cold tongue (i.e., anomalously warm Niño 3 and Niño 3.4 SSTAs), then the SST and thus SLP gradients would weaken (i.e., the Southern Oscillation Index would decrease). In turn, the equatorial easterlies would subside, leading to more warming of SST and eventually a shift in the Walker Circulation such that the convection appears over the now anomalously warm central and possibly eastern Pacific. Conversely, an initial cooling of SST could lead the system in the opposite direction, resulting in a state with cooler SST over the cold tongue, a stronger SLP gradient, and an upward branch of the Walker Circulation that is more tightly confined to the western Pacific.

Although the existence of these feedbacks is generally well accepted by the scientific community, assessing the state of the system is complicated by the fact that observations are subject to modes of variability other than those described above. This complication is known to lead to ambiguity in assessing the state of the system; for example, it is well known that the traditional ENSO indices based on SLP and SST (SOI, Niño 3, Niño 3.4) do not always vary consistently with each other (e.g., Deser and Wallace, 1987).

We here revisit the supra-seasonal variability of the equatorial Pacific as revealed by OLR observations. OLR data is a known proxy for deep atmospheric convection and has been available reliably since 1979, and as far back as 1974. OLR observations have confirmed that the equatorial Pacific undergoes large intraseasonal and interannual variability in deep convection. By averaging over space and time it is possible to focus on interannual variability. We here offer perspective on interannual anomalies of the equatorial Pacific by looking at monthly and spatially averaged OLR values over three regions that collectively span much of the central and western basin. Results are compared to other traditionally used information (e.g., SSTA and SLP).

Section 2 describes the data sets used. Section 3 discusses various monthly averaged time series. Section 4 examines the distributions of monthly average values. Section 5 presents statistical analysis of the distribution of annual peaks. Section 6 discusses the implications of these results. Section 7 presents some conclusions.

2. Data and Methods

We use the daily "Interpolated OLR" data provided by the NOAA/OAR/ESRL PSD, Boulder, Colorado, USA, from their web site at `http://www.cdc.noaa.gov/`. Following several previous studies (e.g., Garreaud and Wallace, 1997; 1998), we consider a convective index (CI) defined as 230-OLR. Positive values of this index are generally considered to be indicative of deep convection. We use monthly averaged OLR values, spatially averaged over the three regions listed in Table 1. The longitude boundaries of the two central Pacific regions can be varied by 10 degrees without significantly af-

Table 1: OLR analysis regions.

Region Name	Latitude Range	Longitude Range
Eastern Central Pacific (ECP)	155°W to 125°W	4°S to 4°N
Western Central Pacific (WCP)	175°E to 155°W	4°S to 4°N
Western Pacific (WP)	150°E to 180°	5°S to 5°N

fecting the results presented here. Results for the western Pacific region are more sensitive to such changes, although they remain qualitatively similar.

We also use ENSO indices obtained as follows; SST data was provided by the Hadley Centre's HadISST data set (Rayner *et al.*, 2003, available at `http://hadobs.metoffice.com/hadisst/`). Anomalies were determined as the difference between monthly averages and the monthly mean climatology (base period January 1971 to December 2000), consistent with current practices. SSTA was then averaged spatially over the standard Niño 3 and Niño 3.4 regions (150°W–90°W, 5°S–5°N and 170°W–120°W, 5°S–5°N, respectively).

Monthly averaged values of the Troup Southern Oscillation Index, based on SLP at Tahiti and Darwin, were obtained from the Australian Bureau of Meteorology. This data is available at `http://www.bom.gov.au`. We here use a Jan 1971 to Dec 2000 base period, for consistency with the SST-based indices.

Monthly averages of the Multivariate ENSO Index (MEI) were obtained from NOAA's ESRL website. This index is based on the covariance of six variables observed over the tropical Pacific (sea-level pressure, zonal and meridional components of near surface winds, SST, near surface air temperature and cloud fraction, Wolter and Timlin, 1998). Data is presented as provided, based on a reference period of 1950–1993.

We also determine the monthly average Bjerknes ENSO Index (BEI, Harrison and Larkin, 1998) from the near real-time International Comprehensive Ocean-Atmosphere Data Set (ICOADS) data provided by the NOAA/OAR/ESRL PSD, Boulder, Colorado, USA, from their web site at `http://www.cdc.noaa.gov/`. BEI is based on the sum of (–1 × normalized eastern equatorial Pacific SLP anomaly), (normalized eastern central equatorial zonal wind anomaly), and (–1 × normalized eastern Inter Tropical Convergence Zone meridional wind anomaly). A base period of January 1971–December 2000 was used for anomaly determination. BEI3, the 3-month running average version, is also considered. In this case, normalization is done after applying the running-mean filter.

3. Results

We focus first on monthly averaged CI over the Eastern Central Pacific (ECP), where CI values are most often (about 85% of the time) below -20 W m^{-2}, indicating that arid conditions persist in the ECP through-

out most years (Fig. 1a). ECP CI typically shows a strong seasonal cycle (see Fig. 1a), in which seasonal minima of about -50 W/m^2 are usually seen in the months of August or September and maxima, ranging from -35 to -20 W m^{-2}, occur in either March or April of each year. Convective activity during four interannual periods (the large events of 1982/1983, 1986/1987, 1991/1992, and 1997/1998), however, was quite different from this usual behavior. In these four events, ECP CI reached levels more typical of the west Pacific (discussed below), and even crossed into the deep convective (CI > 0) regime during the three largest events of 1982/1983, 1991/1992, and 1997/1998 (monthly average values during the 1986/1987 event fall just shy of 0, though weekly averages (not shown) do cross this threshold).

It is notable that these four years are commonly agreed to be warm-ENSO years, and that the areas under these four peaks are qualitatively consistent with the generally agreed upon relative size of the ENSO events (e.g., the 1982/1983 and 1997/1998 events are larger than the 1986/1987 and 1991/1992 events.) The peak of the smallest of these events (1986/1987) is about 1 standard deviation (σ) above the next highest peak (observed in 1992/1993). Thus, these four events can be clearly identified by visual inspection and a wide range of threshold values can be used to unambiguously distinguish these events from others. We will further examine the statistical significance of these events below, but first compare CI and SSTA indices from other regions.

The convective behavior of the Western Central Pacific (WCP) is similar in many respects to that of the Eastern Central Pacific, but shows some important differences on interannual timescales (cf., Figs. 1a,b). WCP and ECP CI are highly correlated (see Table 2) and, like ECP CI, WCP CI shows a clear seasonal cycle, although the timing and amplitudes of the annual peaks are more variable in the WCP (cf., Figs. 1a,b). Like the ECP, CI averaged over the WCP generally remains negative, indicating that deep convection is unusual, in a regionally averaged sense. Convective events, however, are more common in the WCP than the ECP. For example, the four largest WCP CI peaks, which are roughly coincident with those seen in the ECP, are not the only WCP CI peaks that reach the convective regime (CI > 0 W m^{-2}). Several others with nearly equal amplitude were observed during years in which the ECP exhibited mostly normal behavior. CI peaks in the –10 to +10 W m^{-2} range can be seen in 1989/1990, 1992/1993, 1994/1995, 2002/2003, 2004/2005, and 2006/2007.

Compared to the regions discussed above, a considerably different sort of behavior has been observed over the western Pacific (WP), where CI shifts between the convective (CI > 0) and non-convective (CI < 0) regimes, spending roughly equal time in each, during the period considered (Fig. 1). Although there are numerous occasions when CI is more than ± 1 standard deviation from the mean (dashed lines in Fig. 1), it is difficult to determine if and when anomalies are of interannual timescale because of the relatively strong variability at shorter timescales. For this index, visual inspection alone leads to no clear means of unambiguously detecting strong interannual anomalies of the type seen in ECP CI.

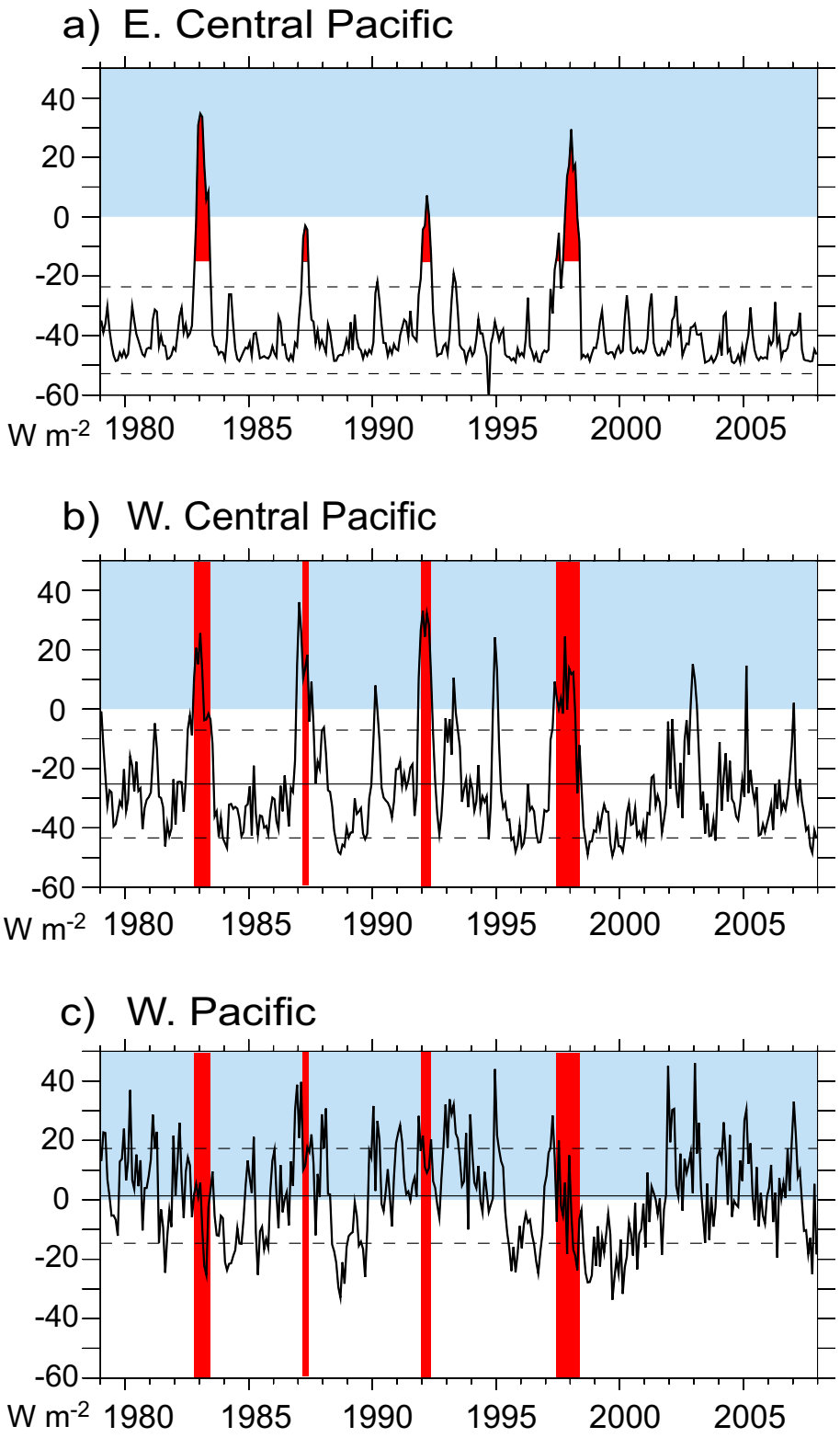

Figure 1: Tropical Pacific OLR-based convective indices.

Table 2: Cross-correlation coefficients of the monthly-average indices considered here.

	WCP	**WP**	**Niño 3**	**Niño 3.4**	**MEI**	**BEI**	**SOI**
ECP	0.68	0.15	0.69	0.56	0.64	0.68	–0.47
WCP	—	0.63	0.74	0.77	0.76	0.58	–0.63
WP	—	—	0.35	0.45	0.44	0.18	–0.43
Niño 3	—	—	—	0.94	0.91	0.78	–0.64
Niño 3.4	—	—	—	—	0.93	0.65	–0.72
MEI	—	—	—	—	—	0.71	–0.79
BEI	—	—	—	—	—	—	–0.51

In some respects, there is considerable agreement between cold-tongue SSTA and the central Pacific CI indices discussed above (cf., Figs. 1 and 2a,b). Of the time series considered, the highest OLR/SSTA correlation is between Niño 3.4 and WCP CI (see Table 2). There is generally good agreement between the timing and amplitudes of peak events seen in these two time series (cf., Figs. 2a and 1b). Thus, a relatively consistent picture of coupled tropical Pacific variability develops from the comparison of WCP CI and Niño 3.4 alone.

There is still also much agreement between ECP CI and Niño 3.4 (Fig. 2b), though, on closer inspection, it is clear that the relationship is not a perfect match. Similarities include the fact that the four largest ECP convective events coincide with the largest Niño 3.4 peaks (times when ECP CI > -15 are shown by red shading in Fig. 2). There are, however, several other intervals in which Niño 3.4 is 0.5 to $\approx$1.8 standard deviations warmer than average, yet ECP CI values remain nearly normal (e.g., 1979/1980, 1993/1994, 1994/1994, 2002/2003, 2004/2005, and 2006/2007). Thus, while it is true that all four ECP convective events occur during times of warm SST, the converse does not hold; warm Niño 3.4 SSTA does not necessarily lead to convection in the ECP. This suggests that warm Niño 3.4 SSTA is a necessary but insufficient condition for convection to reach the ECP.

ECP CI and Niño 3.4 also show significant differences in the degree of separation between the largest and more "normal" amplitude peaks. Referenced to their respective σ values, ECP anomalies are larger; the largest four ECP peaks exceed the mean by 2.5 σ and the largest by more than 5 σ, while only two Niño 3.4 peaks are in the 2.5–3 σ range. The number of events that can be unambiguously distinguished by a threshold value is also different for Niño 3.4. Niño 3.4 shows only two peaks (1982/1983 and 1997/1998) that are approximately 1 σ or more above the next highest (1991/1992). There are, however, several other peaks within 1 σ of this third-highest peak (at about 2 σ) in addition to several others above 0.5 σ. Thus, using 1 σ as a rough measure of sufficient separation, only two events can be distinguished from Niño 3.4 unambiguously.

From the perspective taken here, Niño 3 variability (Fig. 2b) resembles that seen in Niño 3.4, and is thus related similarly to central Pacific CI. For instance, the largest Niño 3 and Niño 3.4 peaks occur nearly simultaneously. It is notable, however, that more separation exists between the largest Niño 3

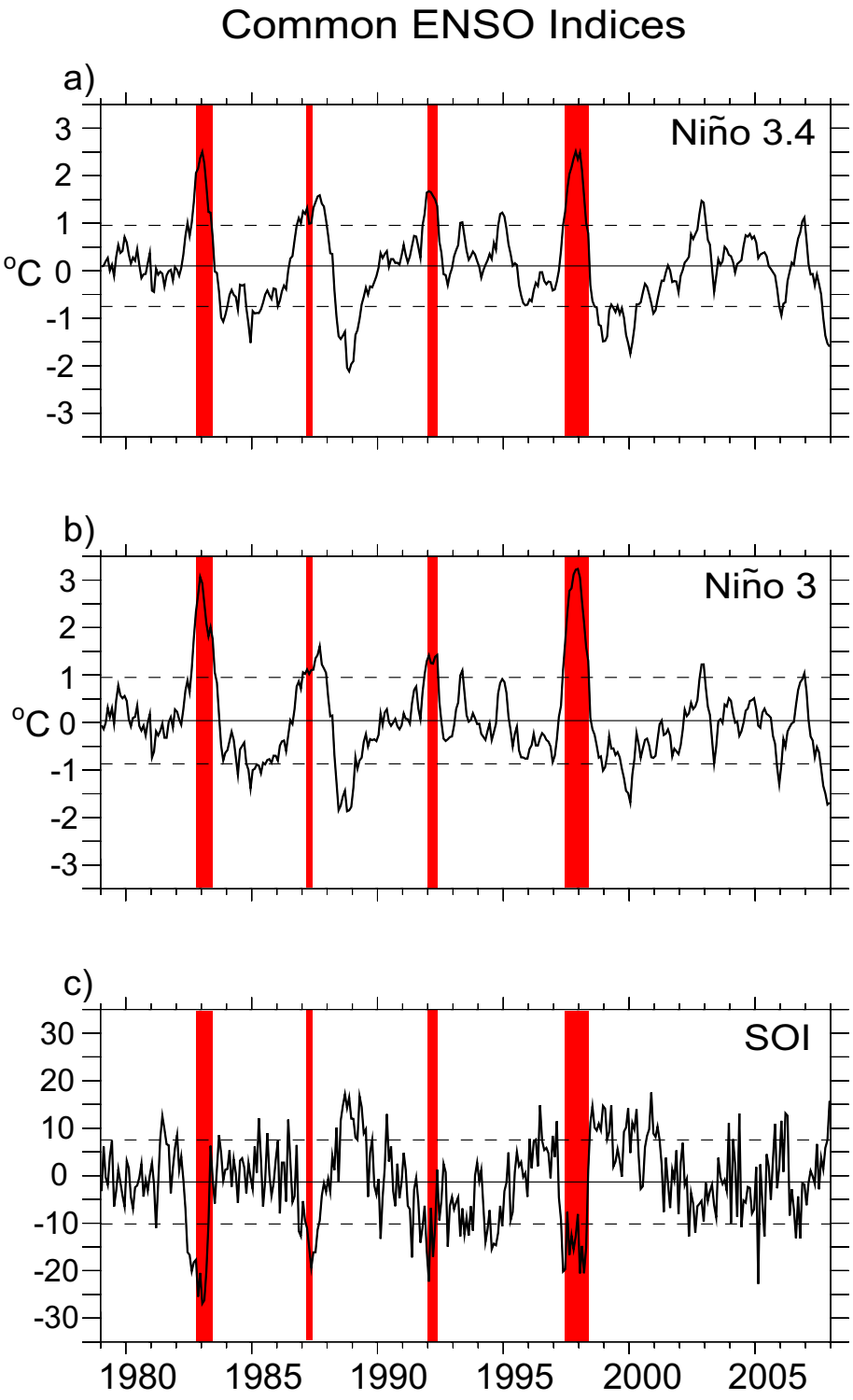

Figure 2: Tropical Pacific SST and SLP based ENSO indices.

peaks and the background variability; however, this separation is not as large as that observed for ECP CI. We will further discuss the distribution of peak Niño 3 values in Sections 4 and 5.

Monthly mean Troup SOI (Fig. 2c) is comparatively noisy, showing more variability at high frequency (near-monthly) than the other time series discussed here. Thus, distinguishing interannual anomalies based on peak (or trough) values is complicated by this relatively strong variability at shorter timescales. Some of the lowest minima in SOI are seen at the times of the four largest ECP peaks discussed above, although other troughs of roughly the same magnitude are also present during other intervals (e.g., 1992/1993, 1993/1994, 2004/2005). SOI is significantly (negatively) correlated with the other time series considered here (Table 2), though discrepancies are apparent and can lead to interpretations of interannual anomalies different from those of SSTA, as has been discussed in previous work (Deser and Wallace, 1987).

Variability of the BEI index (Fig. 3a) appears most closely related to that of Niño 3, and confirms that the events of 1982/1983 and 1997/1998 were the largest warm-ENSO events in the recent past, with substantial events also during 1986/1987 and 1991/1992. It is notable that the BEI is based on surface atmospheric information rather than SST. This agreement thus confirms that, during these intervals, the surface co-varies in a manner similar to that first discussed by Bjerknes.

Variability of the the MEI index (Fig. 3b) closely matches that of the SSTA time series discussed above (see SSTA/MEI correlations in Table 2). The timing and relative size of the four largest MEI peaks are consistent with those of SSTA and the secondary peaks are also qualitatively consistent. The relative peak-to-background separation is also very similar to that of the SSTA indices. For our purposes, therefore, this index presents a view of tropical Pacific variability that is similar to that of the SSTA indices.

4. Distribution of Monthly-Average Index Values

We next examine the distribution of monthly averages about the means of each time series discussed above. To do this, we tabulated the percentage of monthly average values falling into 1-σ-wide bins, centered on the mean. We compare observational results to those expected for a Gaussian-distributed variable with equivalent mean, σ, and (estimated) degrees of freedom. To aid comparisons, the 95% and 5% confidence levels of the respective Gaussian distributions were estimated from Monte Carlo methods for each bin (details given in Appendix A.) Thus, we are able to determine whether or not the number of monthly averages in a given bin is consistent with a Gaussian distribution, and therefore consistent with being driven by the superposition of many random processes.

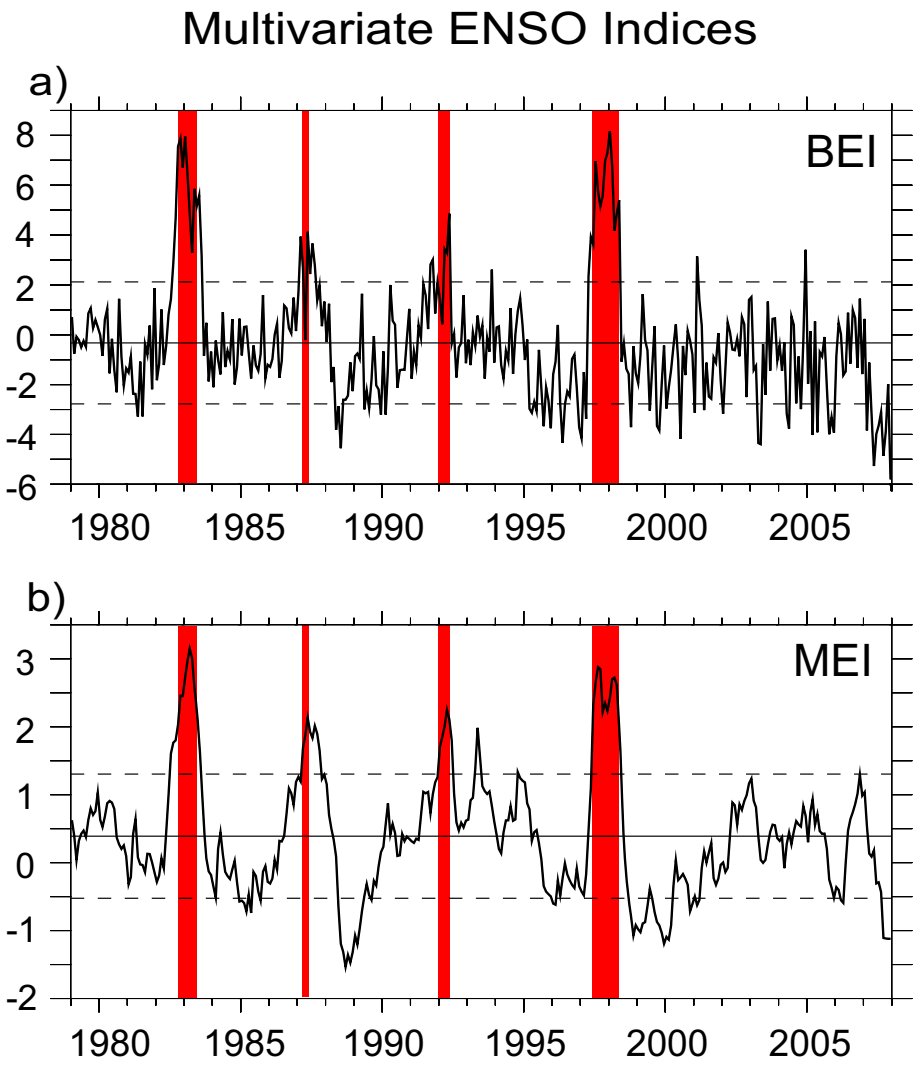

Figure 3: Multivariate ENSO indices (see text.)

It is clear that the distribution of monthly-mean values of ECP CI is non-Gaussian in many respects (cf., Fig. 4a). A significantly larger percentage (about 30%) of ECP CI values are within $\pm 0.5\ \sigma$ of the mean, compared to a Gaussian distribution. The percentage of values in the 0.5- to 1.5-σ range, however, falls short of the Gaussian expectation by about a factor of 3. This relative abundance of values close to the mean aids in making the larger peaks (> about –20 W m^{-2}, or roughly $+1.5\ \sigma$) clearly stand out from background behavior.

Perhaps the most striking features of ECP CI, however, are the amplitudes of the four peaks that extend more than $2.5\ \sigma$ above the mean (i.e., the events of 1982/1983, 1986/1987, 1991/1992, and 1997/1998). Among these events, there are 18 monthly averages above $2.5\ \sigma$. This is more than 10 times the number expected from a Gaussian distribution with equivalent mean and σ. Two observed peaks (a total of 4 months) even exceed the

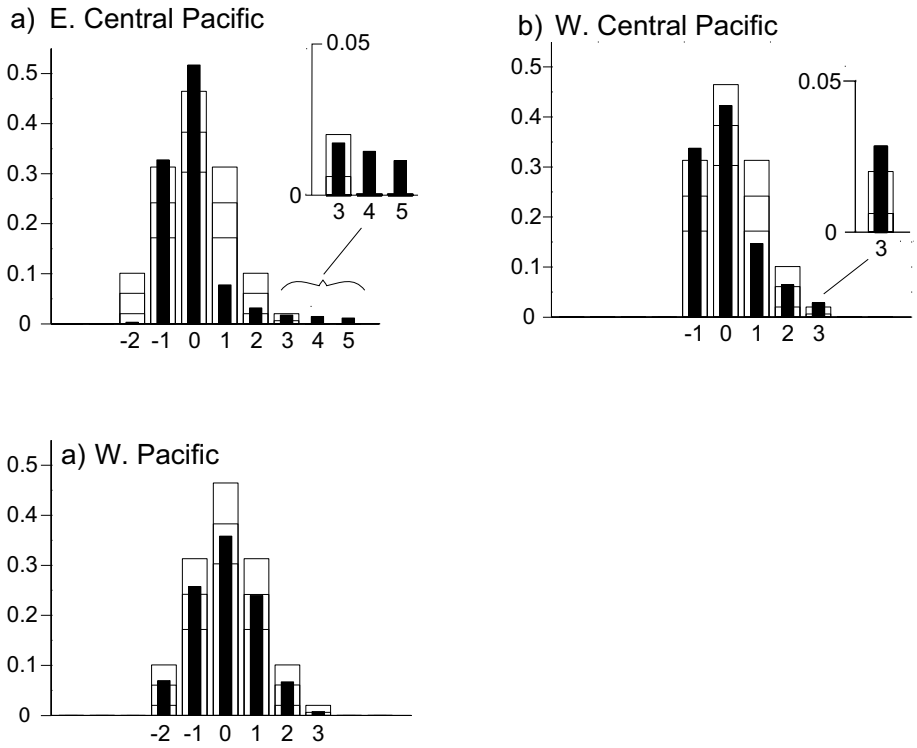

Figure 4: Distributions of monthly-average index values. Bin spacing is 1 σ. Hash marks at expected value and p = 0.05, p = 0.95 levels for a Gaussian-distributed variable with mean and σ equivalent to observations.

mean by 4.5 σ. This is highly inconsistent with a Gaussian distribution; a time series that follows a commensurate Gaussian-distributed time series would have to be about 7000 times as long as the one considered here to be expected to include just two values above 4.5 σ.

The distribution of monthly averages of WCP CI (Fig. 4b) is similar, in some respects, to the ECP distribution. Like the ECP, there is a relative (to Gaussian) enhancement of values in the –1 and 0 σ bins and a relative scarcity of values in the +1 σ bin, though this is more moderate in the WCP case (cf., Figs. 4a,b). The abundance of values in the +3 σ bin slightly exceeds the 95% limit in the WCP case, as it nearly does in the ECP case. Unlike ECP, however, no values are seen above this bin in the WCP case. Thus, while the asymmetry of this distribution is clearly non-Gaussian, this result suggests that only moderate statistical significance can be attached to any specific feature.

The distribution of monthly averages of WP CI (Fig. 4c) is consistent with results from a Gaussian distribution for each bin.

The Niño 3 SSTA and WCP CI distributions share many of the same characteristics, although the Niño 3 distribution is somewhat closer to a Gaussian, statistically (cf., Figs. 4b and 5a). Like WCP, the Niño 3 distribution is asymmetrical, with a relative (though less than 95% significant) abundance of values in the –1 and 0 σ bins. There is also a relative, marginally significant deficit of values in the +1 bin. The +2 and +3 σ

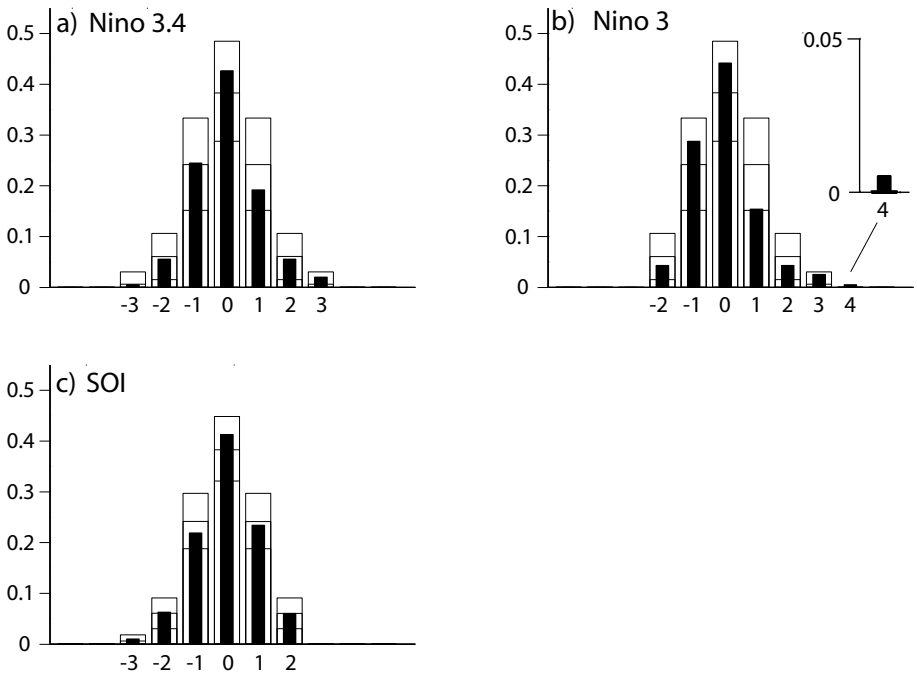

Figure 5: Same as in Fig. 4, except for indices as listed.

bins are filled, respectively, less and more than a pure Gaussian distribution would have them, but these discrepancies are within the 5% and 95% confidence intervals (Fig. 5a). The lone Niño 3 result, from this analysis, that exceeds the 95% confidence interval is the percentage of values in the +4 σ bin. This threshold (3.5 σ) was crossed in only 2 months, both during the 1997/1998 event (the peak of the 1982/1983 event is between 3.3 and 3.4 σ).

It is interesting that the remaining distributions of monthly average values Niño 3.4 and Troup SOI are consistent with results from a Gaussian distribution for each bin/data set combination considered here (Figs. 5b,c), as is the MEI index (Fig. 6b). This suggests that detecting any particular signal of interest from these indices will be difficult because of the relatively high level of variance contributed by other processes.

The BEI index shares some of the characteristics of the ECP and WCP indices. For example, the number of values falling in the 0 σ bin is relatively high, while the +1 σ bin is rather sparsely populated. The statistical significance of these features, however, is considerably less than that of the ECP CI case. Still, as for the ECP and WCP indices, some BEI values exceed the +3 σ bin, which is inconsistent with BEI being a Gaussian-distributed variable.

In summary, in this section we effectively examined the potential signal-to-noise relationship for each of the time series considered here by comparing the distributions of observed monthly averages to expectations for commensurate Gaussian distributions. Results show that the prospects for detec-

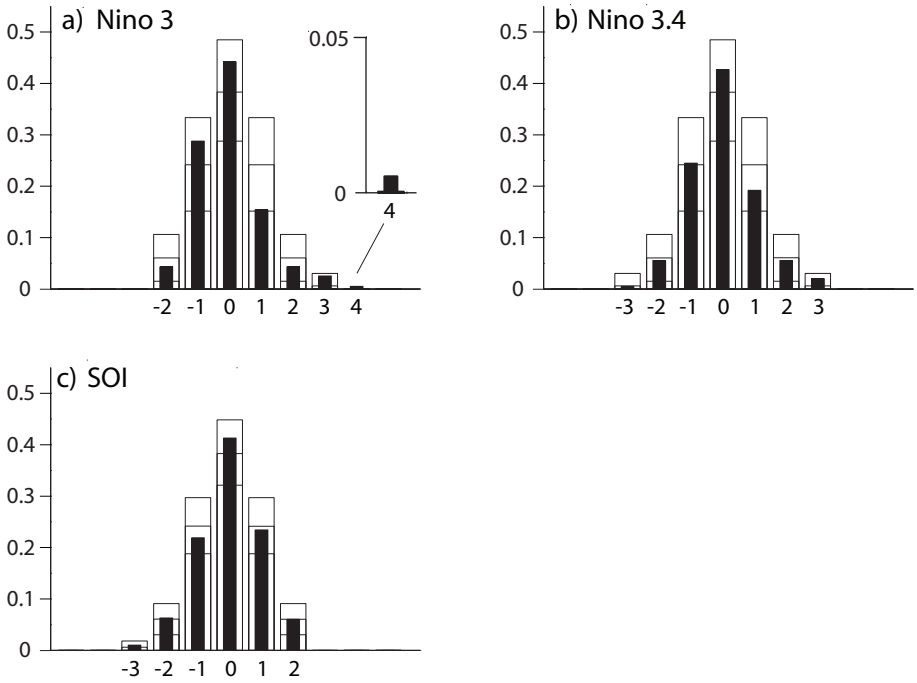

Figure 6: Same as in Fig. 4, except for indices as listed.

tion of significant peak-events are good for ECP CI, moderate for WCP CI, Niño 3, and BEI, and poor for the other time series, including Niño 3.4.

5. Distribution of Annual Peaks

Because of the current focus on interannual anomalies of the tropical Pacific, in this section we consider the distribution of annual peaks among several of the indices discussed here; the four that showed good or moderate potential for event detection in the analysis presented above (ECP CI, WCP CI, BEI, and Niño 3.4), and two others (Niño 3 and SOI) that did not, but are generally referred to when considering interannual anomalies of the tropical Pacific system. The analysis discussed here expands upon results presented above by including results that are dependent on the temporal distribution of peaks on interannual timescales.

Here, we analyze rank-ordered profiles of annual peaks from each index. Annual peaks were found by selecting the maximum monthly average value within each October (Year 0) to September (Year +1) annum of the 1979 to 2007 period (28 peaks in all.) This October to September annum was chosen to be consistent with the climatological minimum in tropical Pacific CI, though shifting the interval by a few months does not significantly affect the results.

When plotted in rank order (see Fig. 7a), it can be seen that most of the ECP CI annual maxima (rank order 1–23) fall within 1.4 σ of the index mean (the average over all months in the January 1979–September 2007 period).

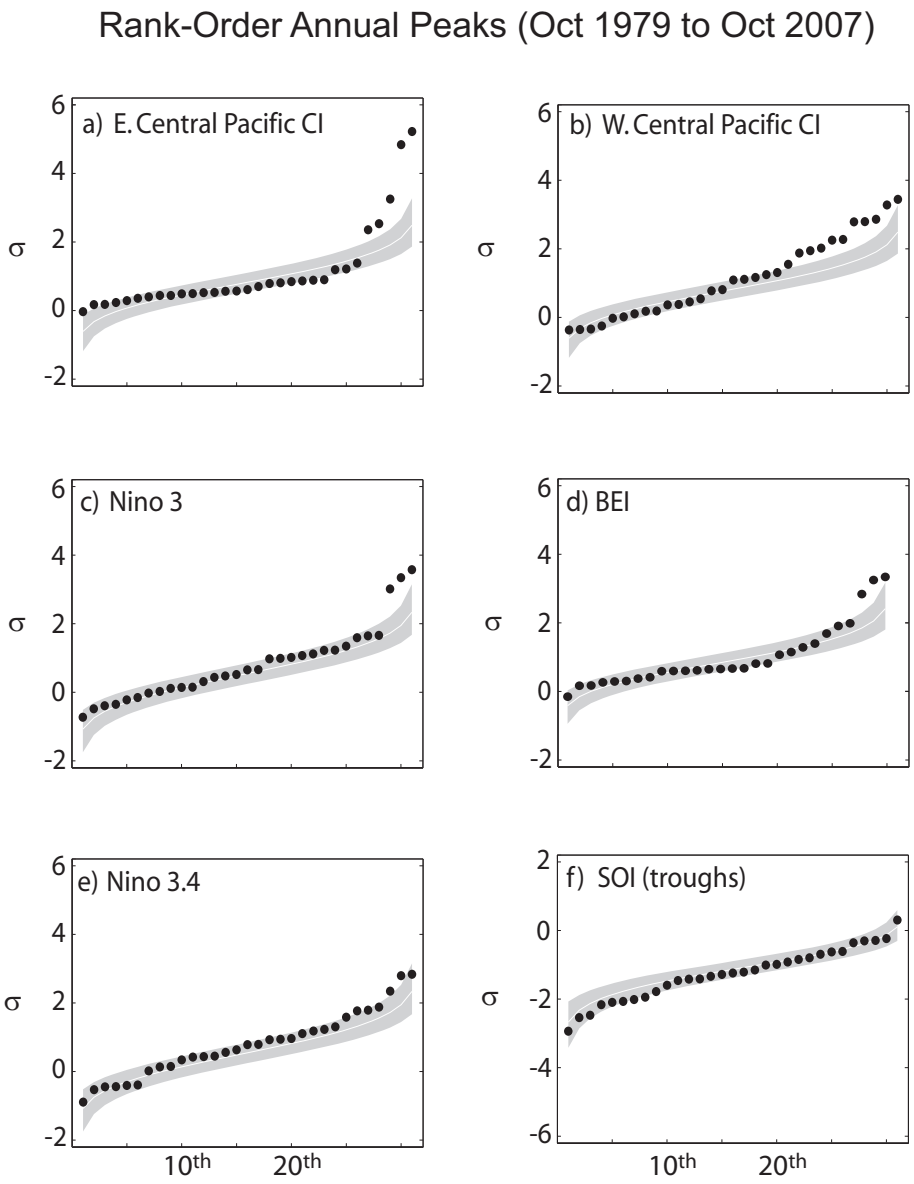

Figure 7: Rank-order annual peaks (October year 0 to September year +1) of OLR/ENSO indices (black circles). Gray shading is for the $0.05 <$ probability < 0.95 levels for a Gaussian-distributed variable with the same mean and σ as observations. The white line is the expected value for a Gaussian-distributed variable.

In this range, peak-to-peak increments are relatively small and uniform, especially between the 2nd- and 20th-ranked peaks, which are separated in a nearly linear manner by increments of $<0.1\ \sigma$. A break from this uniformity is seen between the 23rd- and 24th-highest peaks, which are separated by nearly $1\ \sigma$. Each of the next four highest peaks are more than $2.5\ \sigma$ above the index mean and the highest extends to more than $5\ \sigma$ (as discussed above).

In order to gage the significance of any given annual peak ECP CI value, we have calculated the 5% and 95% confidence intervals for the rank-order of

Table 3: Statistics of 1979–2007 OLR/ENSO indices.

Region	Mean	σ	Deg. Freedom/Year
ECP	–38.21 (W m^{-2})	14.6 (W m^{-2})	3
WCP	–25.2 (W m^{-2})	18.16 (W m^{-2})	3
Niño 3	0.04 (°C)	0.91 (°C)	2
Niño 3.4	0.10 (°C)	0.85 (°C)	2
SOI	–1.33	8.85	5
BEI	–0.33	2.45	4

annual peaks for a Gaussian-distributed variable with mean and σ equivalent to observations (details given in Appendix, values in Table 3).

When plotted against these confidence intervals, it is clear that the values of the five largest annual peaks in ECP are significantly above the 95% confidence interval. It is also interesting that the remaining, lower ranked, annual peak values are distributed somewhat more linearly that predicted by the Gaussian distribution. This highlights the remarkable consistency of the seasonal cycle of ECP CI that is seen during most years.

It is notable that the 5th-highest ECP CI peak occurs in the October 1996 to September 1997 interval, as part of the run-up to the large 1997/1998 event (i.e., all monthly-mean values between the 1996/1997 and 1997/1998 peaks are more than 1 σ above the mean). Thus, the five largest peaks selected by the methods used here are each associated with the four large ECP CI events discussed above.

The four largest WCP CI peaks roughly coincide with the four largest ECP CI peaks. In addition to these, several of the next largest WCP CI peaks exceed the 95% confidence interval, although by a smaller margin than seen in the ECP (Fig. 7b). This is broadly consistent with the results of the distribution analysis, presented above, which showed that, compared to the ECP, WCP CI has a relative abundance of values in the 2- and 3-σ bins, but no values that exceed 3.5 σ. It is notable that this result, which accounts for the temporal spacing of the WCP CI peaks, confers more significance on these secondary WCP peaks (those that do not coincide with the four largest ECP events) than is evident from the results of Section 4 alone. In this case, all peaks that exceed the mean by about 1.5 σ are statistically significant. It is interesting that this corresponds roughly to the deep convection regime, and thus suggests that events in which convection is seen over the WCP region (at monthly or longer timescales and in a regionally averaged sense) are statistically significant anomalies of the coupled tropical Pacific system.

In the case of Niño 3 SSTA, only the three largest annual peaks selected by the method used here exceed the 95% confidence interval (Fig. 7c). Of these, two (the highest and third highest) occur during the large 1997/1998 event that peaks in December of 1997. Thus, we find that only two interannual timescale Niño 3 SSTA events are statistically significant (1982/1983 and 1997/1998.) This result is similar in many respects to that of the BEI index, which also shows the three highest-ranked peaks to be above the 95%

level. Also in this case, these three peaks are associated with what are nominally the 1982/1983 and 1997/1998 events.

It is interesting that the largest annual peak (that of the 1997/1998 event) in the Niño 3.4 record (see Fig. 7e) is not found to be statistically significant by the methods used here, although marginal significance is obtained by the annual peak associated with the second largest event (1982/1983). This result is consistent with results of the distribution analysis described above, which showed that the behavior of Niño 3.4 SSTA is generally consistent with a Gaussian distribution. This confirms results presented above which suggested that using Niño 3.4 SSTA to detect significant and unambiguous interannual anomalies is, at best, problematic because the variability of this index is largely consistent with Gaussian-type behavior, i.e., being driven by the super-position of many random processes.

The behavior of the SOI index is also very close to that expected from a variable that follows a Gaussian distribution (Fig. 7e). Thus it is difficult to attach statistical significance to any given feature of this time series. Note that in this case we have chosen to plot the annual minima rather than maxima, due to the inverse relationship between SOI and the other indices considered.

6. Discussion

By comparing regional averages of monthly OLR and SSTA, we find that years with anomalously warm equatorial SST have three distinctive types of OLR behavior. The first class involves eastern central Pacific OLR values characteristic of the western Pacific. The second class involves western central Pacific events with peak values about half as anomalous and of substantially shorter duration. The third class involves only very weak OLR anomalies over these regions. In fact, the third class of events does not stand out above the normal year-to-year variability in any clear way. The first class of events corresponds with the subset of years most commonly identified as El Niño years (1982–83, 1986–87, 1991–92, 1997–98). The Second Class events (1989–90, 1992–93, 1994–95, 2002–03, 2004–05, 2006–07) have been noted as anomalous relative to particular ENSO indices but are less widely agreed to be El Niño years. The Third Class events (1979–80, 1980–81, 1987–88, 2001–02, 2003–04) include some years that have not been considered El Niño years.

The second class of events, which have many characteristics of a full-blown El Niño, but do not evince convective conditions in the eastern central Pacific, are intrinsically interesting and may warrant special consideration in their own right, as a better understanding is formed of the affects that this second class of anomalies may have on global weather anomalies. Unfortunately, rigorous studies along these lines are hampered because only a few such events have been observed in the recent, satellite era.

A common characteristic of the first class of events is a shift in the climate of the eastern central Pacific from arid to convectively active regimes. This

shift is a significant phenomenological change in the air-sea coupling of the tropical Pacific that has implications for global weather anomalies. It is also straightforward to detect operationally and stands out unambiguously from the normal levels of variability inherent to OLR measured over the eastern central Pacific. Since Bjerknes feedbacks are clearly active in these events (e.g., anomalously low SOI and warm cold-tongue SSTA), and since they occur during the years most commonly agreed to be El Niño years, we propose that these events be distinguished from the others.

We believe it is in the interest of the broader scientific community to reserve the name "El Niño" for years in which the monthly averaged eastern central Pacific convective index (230-OLR) is observed to exceed –15 W m^{-2}. This is because it is the global weather anomalies associated with ENSO variability, not the state of the tropical Pacific itself, which is of the broadest importance to society. Because the teleconnections that sustain such weather anomalies are triggered by the shift of convection from the west to the central Pacific, we believe this convention is best ensured to preserve the relationship between weather anomalies and El Niño that has been documented previously (see Larkin and Harrison, 2005a;b).

7. Conclusion

Our analysis of various monthly mean ENSO-related indices has shown that OLR averaged over the Eastern Central Pacific is unique in terms of its ability to clearly and unambiguously distinguish anomalous behavior of the coupled ocean-atmosphere tropical Pacific system on interannual timescales. This metric clearly shows that the years most commonly agreed to be El Niño years, 1982/1983, 1991/1992, 1986/1987 and 1997/1998 stand out from the rest in terms of convective phenomenology.

We believe it makes good sense to distinguish these years from others that have been related to ENSO by some indices, but do not show convection over the eastern central Pacific. Such practice, we believe, is most likely to preserve the previously documented relationship between ENSO variability and global weather anomalies that has become well known outside of the scientific literature. This is because the teleconnections involved in allowing the weather anomalies to persist are driven by the shift in convection from the west to the eastern Pacific.

Since the OLR-based indices discussed here are defined in an absolute sense, and are little affected by long-term surface temperature trends, the use of these indices would alleviate biases due to changes in the mean climate of the tropical Pacific, as may occur due to the increased levels of anthropogenic CO_2 in the atmosphere, or may stem from decadal or longer-term natural variability.

Because the OLR-based El Niño index discussed here is simple to use and evaluate, does not depend on specification of climatological conditions, and is derived from monthly means, it is suitable for use as an operational definition of this phenomena. In some cases, the SSTA-based definitions

currently in place give an earlier alert that an ENSO event is likely to occur. Since this is useful information, but warm SSTA does not always lead to a shift in convection over the cold tongue, we propose that these SSTA (and SLP) indices be retained and monitored. These can provide an ENSO alert that will persist until either anomalous conditions subside, or an El Niño event is confirmed by OLR information.

8. References

Bjerknes, J. (1969): Atmospheric teleconnections from the equatorial Pacific. *Mon. Weather Rev.*, *97*, 163–172.

Deser, C., and J.M. Wallace (1987): El Niño events and their relationship to the Southern Oscillation: 1925–1986. *J. Geophys. Res.*, *92*(C13), 14,189–14,196.

Garreaud, R.D., and J.M. Wallace (1997): The diurnal march of convective cloudiness over the Americas. *Mon. Weather Rev.*, *125*, 3157–3171.

Garreaud, R.D., and J.M. Wallace (1998): Summertime incursions of Midlatitude air into subtropical and tropical South America. *Mon. Weather Rev.*, *126*, 2713–2733.

Harrison, D.E., and N.K. Larkin (1996): The COADS sea level pressure signal: A near-global El Niño composite and time series view, 1946–1993. *J. Climate*, *9*, 3025–3055.

Harrison, D.E., and N.K. Larkin (1998): El Niño-Southern Oscillation sea surface temperature and wind anomalies, 1946–1993. *Rev. Geophys.*, *36*(3), 353–399.

Larkin, N.K., and D.E. Harrison (2005a): Global seasonal temperature and precipitation anomalies during El Niño autumn and winter. *Geophys. Res. Lett.*, *32*, L16705,doi:10.1029/2005GL022860.

Larkin, N.K., and D.E. Harrison (2005b): On the definition of El Niño and associated seasonal average U.S. weather anomalies. *Geophys. Res. Lett.*, *32*(13), L13705,doi:10.1024/2005GL022738.

Rayner, N.A., D.E. Parker, E.B. Horton, C.K. Folland, L.V. Alexander, D.P. Rowell, E.C. Kent, and A. Kaplan (2003): Global analyses of sea surface temperature, sea ice, and night marine air temperature since the late nineteenth century. *J. Geophys. Res.*, *108*(D14), 4407,10.1029/2002JD002670.

Ropelewski, C.F., and M.S. Halpert (1987): Global and regional scale temperature patterns associated with the El Niño/Southern Oscillation. *Mon. Weather Rev.*, *115*, 1606–1626.

Ropelewski, C.F., and M.S. Halpert (1996): Quantifying Southern Oscillation-precipitation relationships. *J. Climate*, *9*, 1043–1059.

Smith, S.R., D.M. Legler, M.J. Remigio, and J.J. O'Brien (1999): Comparison of 1997–98 U.S. temperature and precipitation anomalies to historical ENSO warm phases. *J. Climate*, *12*, 3507–3515.

Trenberth, K.E., and J.M. Caron (2000): The Southern Oscillation revisited: Sea level pressures, surface temperatures and precipitation. *J. Climate*, *13*, 4358–4365.

Wolter, K., and M.S. Timlin (1998): Measuring the strength of ENSO events—how does 1997/98 rank? *53*, 315–324.

Appendix A. 1950–2007 ENSO Indices

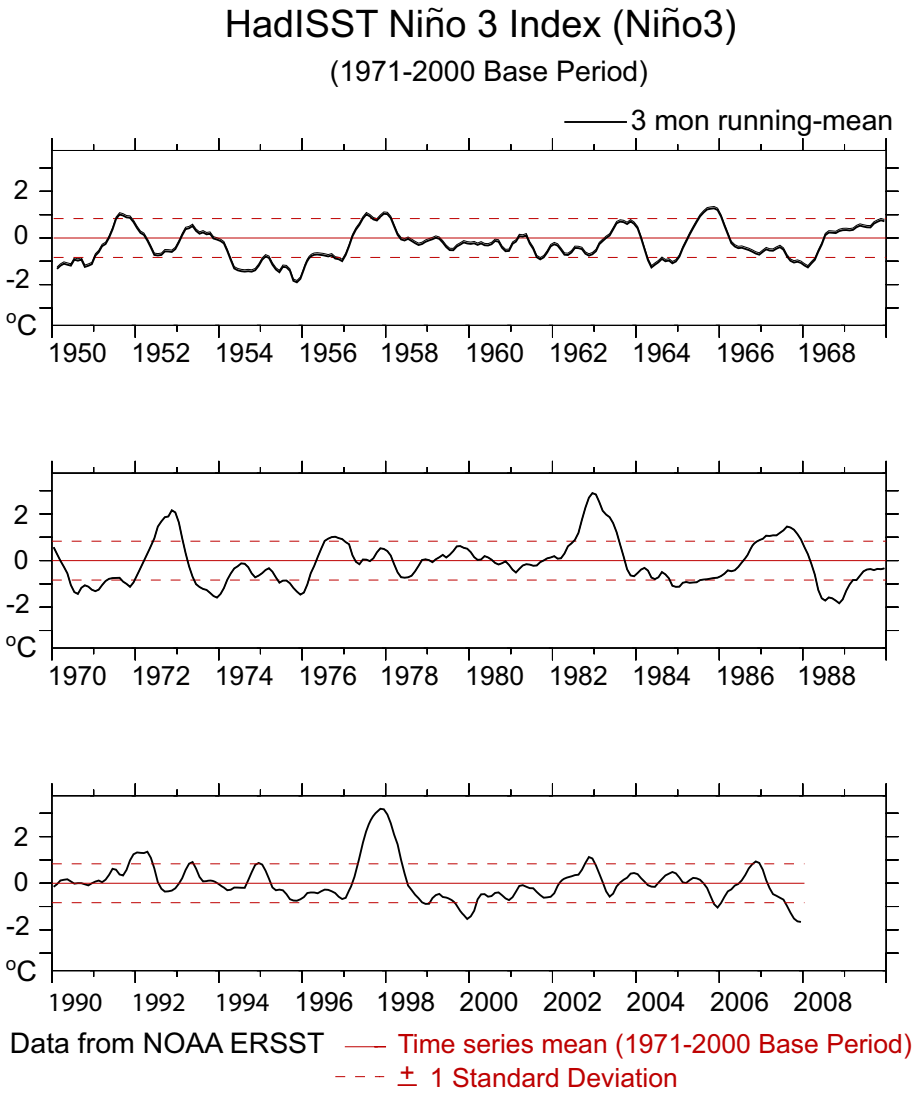

Figure A1: 3-month running mean Niño 3 region SSTA. Data from HadISST.

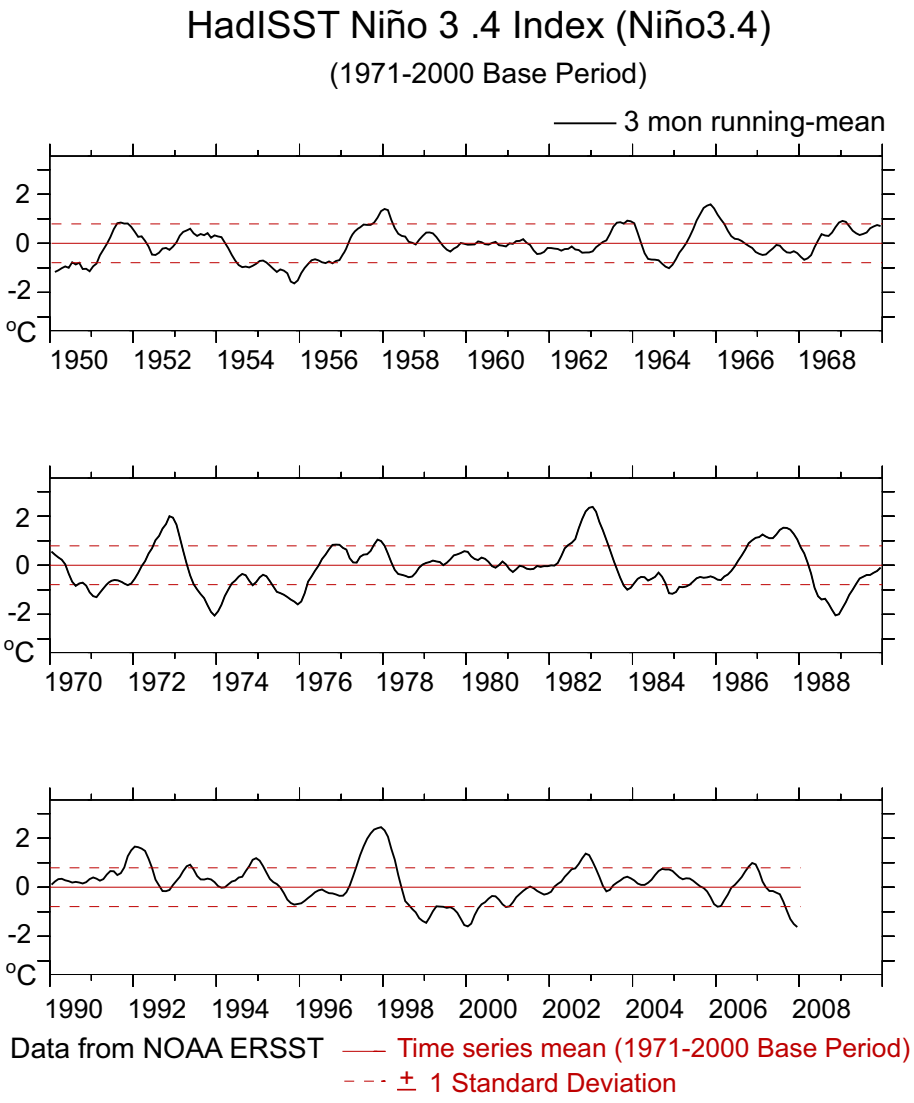

Figure A2: 3-month running mean Niño 3.4 region SSTA. Data from HadISST.

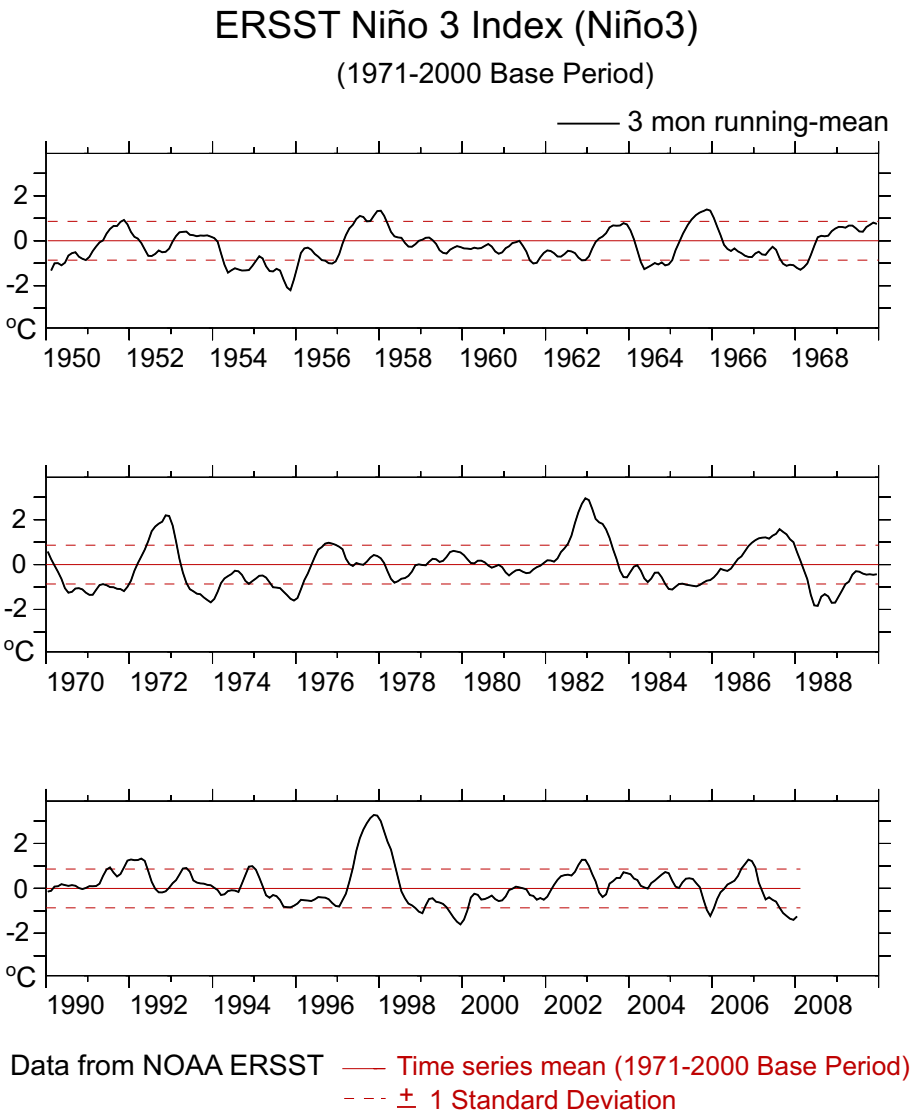

Figure A3: 3-month running mean Niño 3 region SSTA. Data from ERSST.

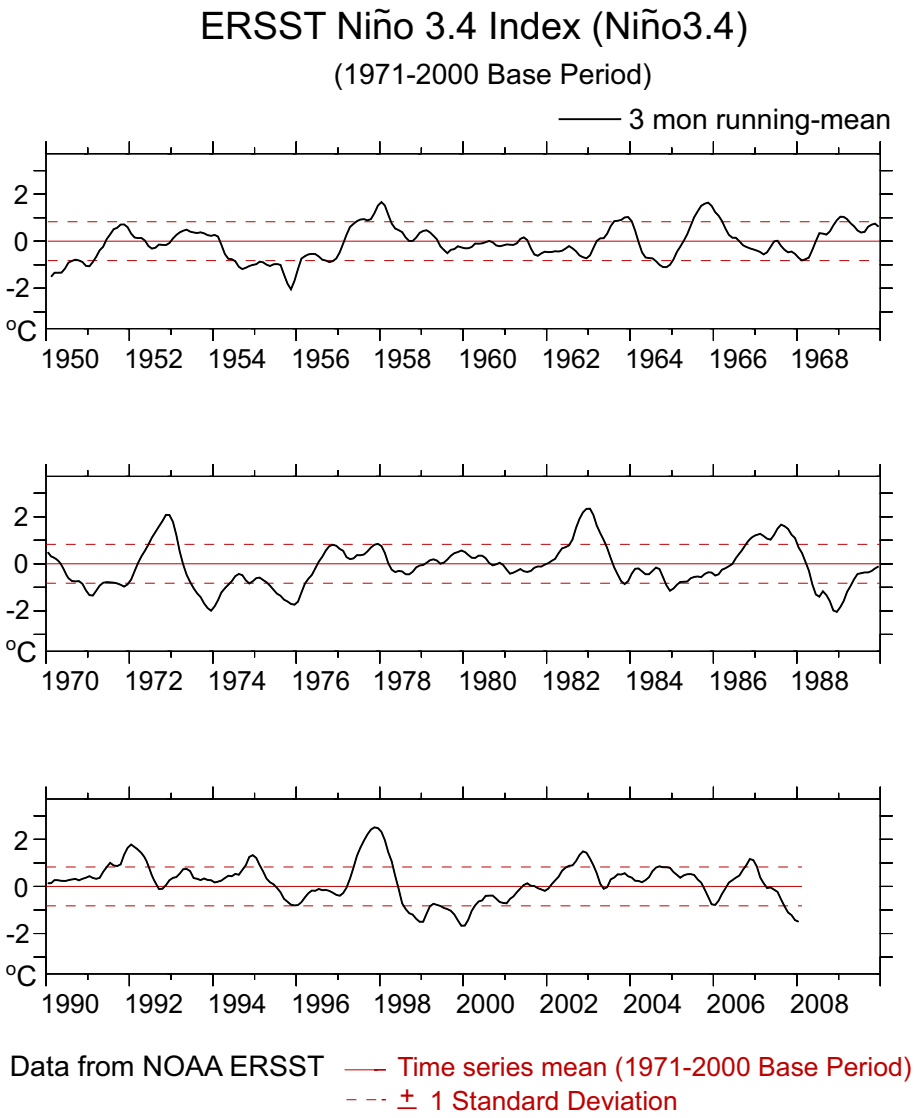

Figure A4: 3-month running mean Niño 3.4 region SSTA. Data from ERSST.

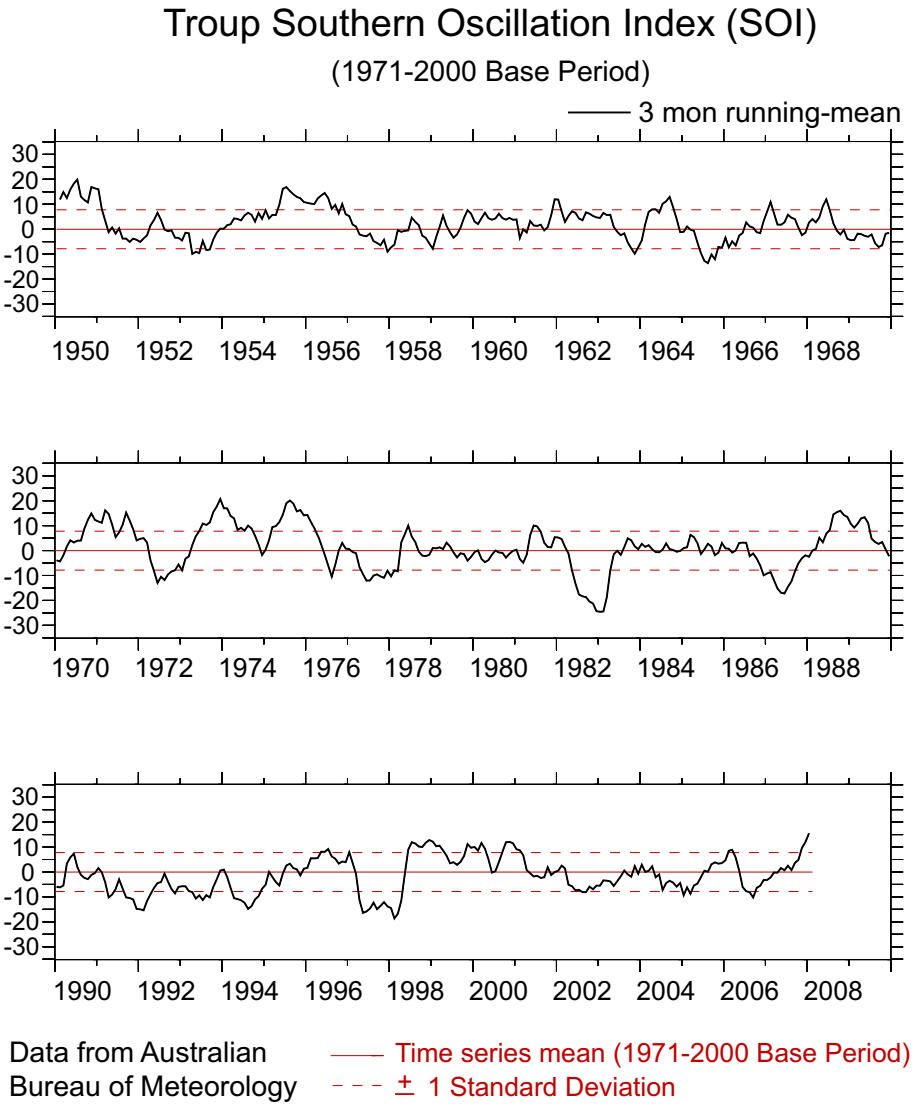

Figure A5: 3-month running mean SOI.

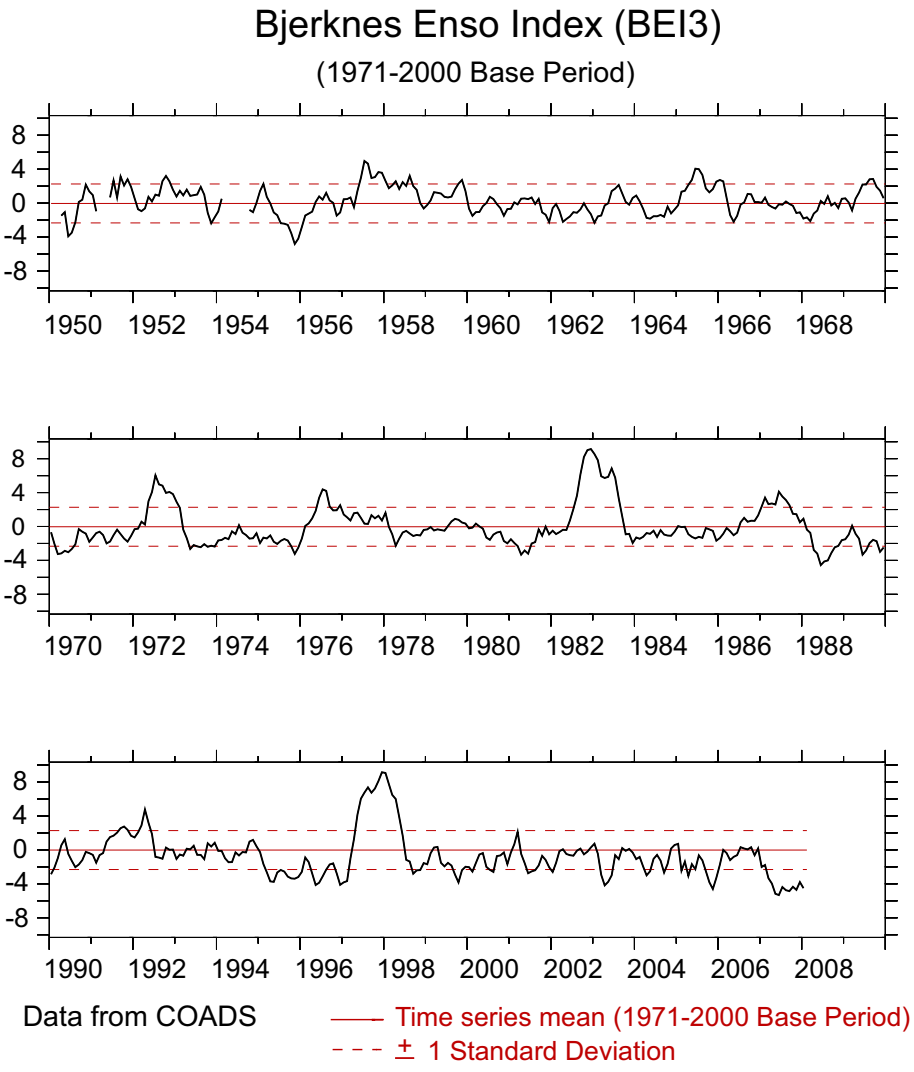

Figure A6: Bjerknes ENSO Index-3. (See Harrison and Larkin, 1998.)

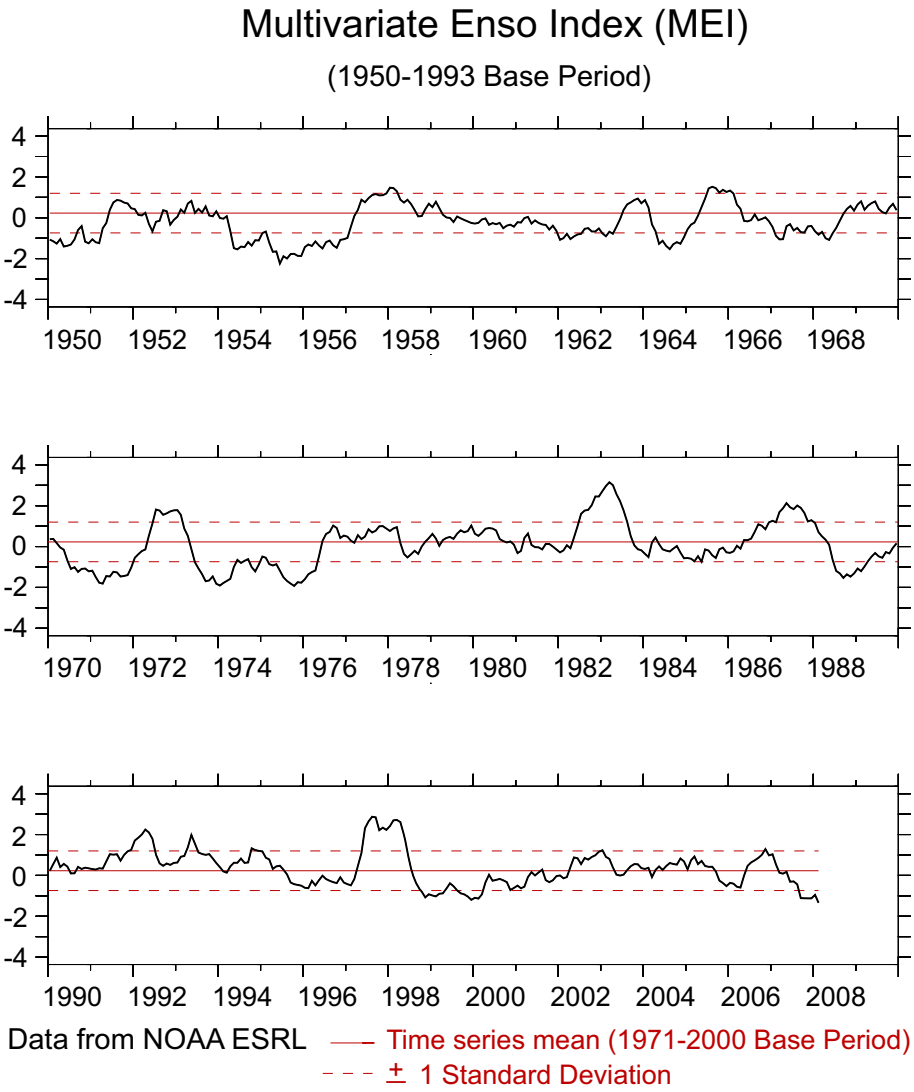

Figure A7: Multivariate ENSO Index. (See Wolter and Timlin, 1998.)

Appendix B. Gaussian Distribution Confidence Intervals

To aid comparison of the distributions of monthly averages discussed above, we compare observed results to those expected from a commensurate Gaussian-distributed variable (see hash-marks in Figs. 4–6). We here describe how the most probable value, 5% and 95% confidence intervals were determined. In this case (for example), the 95% level corresponds to the value that a fundamentally Gaussian process would exceed, on average, in only 1 of 20 chances.

We first calculate the mean, σ, and degrees of freedom contained in each time series (see Table 3). The method for determining the number of degrees of freedom is discussed in Appendix C, although trials have shown that the results, in this case, are not highly sensitive to this value (e.g., qualitatively similar results are obtained when substituting any of the degrees of freedom values used here for another).

Then we generated multiple, hypothetical time series using a Gaussian random number generator (this was done using Matlab's "Randn" function.) We specified that the hypothetical time series be selected from a Gaussian distribution with a mean and σ equivalent to observations. The number of values in each hypothetical time series was set to the number of degrees of freedom contained in the monthly averaged observations, during the 1979–2007 period discussed here (about 350 months in all). A library of 100,000 hypothetical time series was generated for each case.

Each member of this library was then binned according to the procedure used for the observations, then the bin values were sorted in rank order from 1 to 100,000. The average number of values in each bin determines the expected value (middle hash). The 5000th value determines the 5% level and the 95,000th determines the 95% level. Experiment has shown that these levels are stable over multiple repetitions of this process, relative to the differences between the observational results.

Appendix C. Gaussian Annual Peak Rank-Order Confidence Intervals

The confidence intervals for the rank-order profiles discussed herein were determined as follows. For each year of observations (28 in all), we selected X number of values at random from a normal distribution, where X is the number of degrees of freedom per year (listed in Table 3), and the random distribution was specified to have the same mean and σ as monthly averaged observations. The largest of these values (smallest in the SOI case) was then

chosen and saved. Then these "annual peaks" were sorted by magnitude. We repeated this process 100,000 times, saving each result. These results were averaged over rank order to determine the most probable result and sorted by magnitude so that confidence intervals (5th and 95th) could be determined.

The number of degrees of freedom used here was based on a best fit to observational results, with the constraint that an integer number of degrees freedom per year be specified. The values used here are consistent with values estimated from consideration of the time series auto-correlations. Experiment has shown that varying this value by ± 1 degree of freedom/year produces qualitatively similar results, though classification of peaks near the 5% and 95% levels (e.g., $\pm 0.2\ \sigma$) are sensitive to this value.